View metadata, citation and similar papers at core.ac.uk

brought to you by CORE

東北大学機関リポジトリ
TOUR
Tohoku University Repository

Depth Profiling using the glancing-incidence and glancing-takeoff x-ray fluorescence method

著者	Tsuji K., Sato S., Hirokawa K.
journal or publication title	Review of Scientific Instruments
volume	66
number	10
page range	4847-4852
year	1995
URL	http://hdl.handle.net/10097/53256

doi: 10.1063/1.1146163

Depth profiling using the glancing-incidence and glancing-takeoff x-ray fluorescence method

K. Tsuji, S. Sato, and K. Hirokawa
Institute for Materials Research, Tohoku University, Katahira 2-1-1, Aoba-ku Sendai 980, Japan

(Received 30 May 1995; accepted for publication 6 July 1995)

We have developed a new analytical method, which we call the glancing-incidence and glancing-takeoff x-ray fluorescence (GIT-XRF) method. In this method, a fluorescent x ray is measured at various combinations of incident and takeoff angles. A nondestructive depth profiling is possible by using this GIT-XRF method, because the effective observation depth is changed by both the incident and takeoff angles. Here, we introduce the idea of depth profiling using the GIT-XRF method, and then we apply this method to an Au–Si interface reaction. © *1995 American Institute of Physics.*

I. INTRODUCTION

The x-ray fluorescence (XRF) method is mainly used for the bulk analysis of materials. In addition, it has been found that the XRF method with a total reflection phenomenon is a powerful tool for making a trace analysis on a flat substrate.[1–3] This method is called the total reflection XRF (TXRF) method. Furthermore, it has been shown that surface and thin-film analyses are also possible by changing the incident angle. Recently, various types of x-ray fluorescence (XRF) analyses have been developed for surface and thin-film analysis. Three types of XRF methods are categorized with respect to their experimental arrangements as shown Figs. 1(a), 1(b), and 1(c).

The method shown in Fig. 1(a) is the incident angle-dependent x-ray fluorescence (IAD-XRF), or grazing-incidence XRF (GI-XRF) method using a typical TXRF spectrometer. The x-ray detector is set just above the sample, so that the detection angle of the x-ray fluorescence is about 90 deg from the sample surface. The penetration depth of the primary x-ray changes with the incident angle from several nanometers to submicrometers. Thus, thin-film analysis and depth profiling are possible by measuring the incident-angle dependence of the x-ray fluorescence.[4–6]

The second method, shown in Fig. 1(b), is the grazing-exit (or -emission) XRF (GE-XRF) method,[7,8] or takeoff angle-dependent XRF (TAD-XRF) method.[9–11] In this method, the incident angle of the primary x ray is about 90 deg, and the x-ray fluorescence is measured as a function of the takeoff angle. Since the reciprocity theorem is applied in the x-ray region,[12] the same information supplied by the IAD-XRF method has been obtained.[7,12] Another merit of this GE-XRF method is that a two-dimensional analysis of the sample surface is possible by scanning the microbeam of the primary x ray.[13]

The third method, shown in Fig. 1(c), is the glancing-incidence and -takeoff x-ray fluorescence (GIT-XRF) method,[14] which we were the first to develop. Sasaki *et al.* has been developed the refracted x-ray fluorescence (RXF) method[9] or fluorescence x-ray interference (FXI) method.[15] They have measured the x-ray fluorescence only as a function of the takeoff angle. The incident angle of the primary x ray is fixed at a glancing angle where the x-ray fluorescence intensity corresponds to the maximum value. This is because the fluorescent x-ray intensity is strongly dependent upon the incident angle. We utilize the incident-angle dependence in addition to the takeoff angle dependence of x-ray fluorescence intensity. We have previously reported that a surface-sensitive analysis[16] (the first advantage) is possible when both the incident and the takeoff angles are set below the critical angle for total reflection. Furthermore, we can obtain a number of TAD-XRF curves for the various incident angles. Thus, the experimental result is cross checked, and a more accurate thin-film analysis[17,18] (the second advantage) is possible with several TAD-XRF curves.

In this paper, we shall compare the possibility of depth profiling (the third advantage) using the GIT-XRF method and using the IAD-XRF method. The GIT-XRF method is applied to an analysis of the Au–Si interface reaction. The low temperature reaction at the Au–Si interface have been researched by the Rutherford backscattering (RBS) method.[19,20] RBS is a powerful tool for a nondestructive depth analysis, however, the depth information and the elemental information overlap. In addition, the experimental apparatus is expensive and quite large. In contrast, the apparatus for the GIT-XRF method is very simple and inexpensive. The information on the depth profile is obtained independently from the angle dependence of the x-ray fluorescence intensity. Additionally, the GIT-XRF can be measured at atmospheric pressure. We make clear the increased utility of depth profiling using the GIT-XRF method by investigating the well-known Au/Si interface reaction.

II. PRINCIPLES OF GIT-XRF ANALYSIS

In the GIT-XRF method, the x-ray fluorescence intensity is measured as a function of the takeoff angle. The intensity at the glancing-incidence and -takeoff angles can be calculated with a layered model. The calculation procedure has been described elsewhere.[10,11] The density of the surface and the thickness of the thin film are included in the calculation parameters. Figures 2(a) and 2(b) show the density dependence and the thickness dependence of the GIT-XRF profile for a thin Au layer on Si, respectively. Roughly speaking, the peak position is sensitive to the density of the surface layer, and the shape of the GIT-XRF profile is sensitive to the thicknesses of the thin films. The simulated curve is com-

Downloaded 05 Aug 2011 to 130.34.134.250. Redistribution subject to AIP license or copyright; see http://rsi.aip.org/about/rights_and_permissions

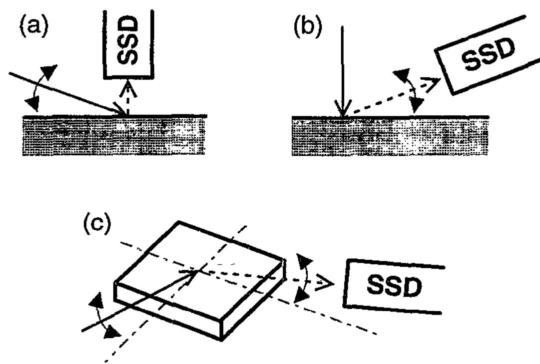

FIG. 1. Experimental arrangements of x-ray fluorescence methods. (a) Incident angle-dependent x-ray fluorescence (IAD-XRF), (b) takeoff angle-dependent x-ray fluorescence (TAD-XRF), and (c) glancing-incidence and -takeoff x-ray fluorescence (GIT-XRF). The solid arrows and the dotted arrows denote the primary x ray and the fluorescence x ray, respectively.

pared with the experimental plots. As a result, we can estimate the thickness or density of the thin films from the calculation parameters which fit the best.

Next, we describe a depth-profile analysis using the GIT-XRF method. Nondestructive depth analysis has previously been studied by using the TXRF method.[21,22] This is based on the principle that the penetration depth of the primary x rays is changed by the incident angle. Therefore, the incident angle dependence of the x-ray fluorescence intensity provides a depth information. Figure 3(a) is an Au (20 nm) thinfilm on an Si substrate. The models in Figs. 3(b) and 3(c) show the different depth profiles of Au in Si. The Au quantities in Figs. 3(a)–3(c) are the same. Figures 3(d)–3(f) show the calculated AD-TXRF curves. The main difference in the curves is found at the incident angle where the x-ray fluorescence intensity begins to increase. This angle corresponds to the critical angle for total reflection. As shown in Fig. 2(a), this critical angle is dependent on the surface density. The surface densities of the depth profile models decrease in the order shown in Figs. 3(a)–3(c). Therefore, the critical angle, shown by arrows in the figures, also shifts to the lower takeoff angle in the same order. However, other clear differences have not been observed. This shows the limitation of the TXRF method in depth profiling.

On the other hand, we can obtain a large number of curves using the GIT-XRF method. Figures 3(g), 3(h), and 3(i) show the GIT-XRF curves for the depth-profile models of Figs. 3(a), 3(b), and 3(c), respectively. The TAD-XRF curves calculated at the incident angles of 2, 3, 4, and 6 mrad are shown in each figure. In the case of the thin-film model in Fig. 3(a), the takeoff angles of the peaks of the four curves do not shift as much. In the case of the depth profile in Fig. 3(b), all the peaks shift to a low takeoff angle due to the decrease in surface density. The shapes of the curves broaden in comparison with those of Fig. 3(g). These differences are due to the difference in the depth profile. In the case of the depth profile of Fig. 3(c), the takeoff angles of the peaks shift to the lower angle. Moreover, the characteristic GIT–XRF profile is observed at an incident angle of 3 mrad. In this depth profile model, a layer with a large density in comparison with the surface density exists at a depth of 30 nm. The penetrating x rays are reflected by this layer, therefore, a large electric field exists above it.

As described above, the GIT–XRF curves give much more information on the depth profile in comparison to the TXRF method. This indicates that the GIT-XRF method has more potential for use in depth profiling.

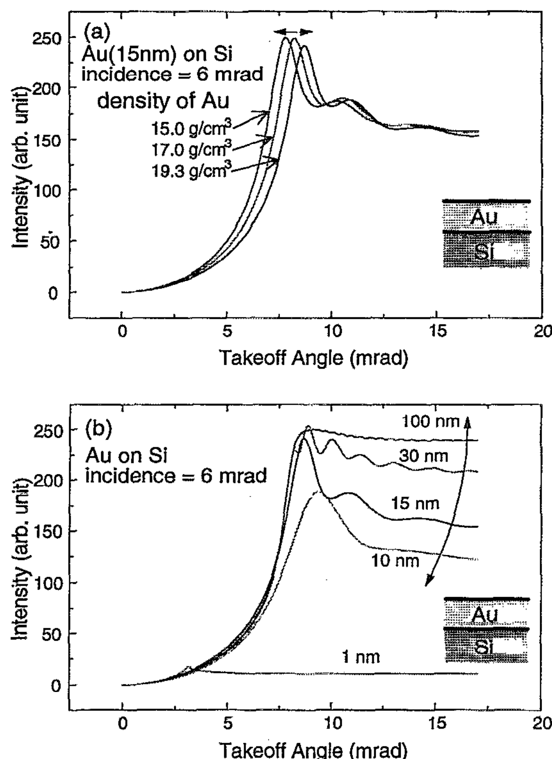

FIG. 2. (a) The density dependency of the TAD-XRF curves at the incident angle of 6 mrad. When the surface density is small, the peak of the curve shifts to the lower angle. (b) The thickness dependency of the TAD-XRF curves at the incident angle of 6 mrad. When the thickness of the thin film increases, the shape of the curve broadens.

III. EXPERIMENTAL DETAILS

A. Experimental setup

The experimental setup of the GIT-XRF method is shown schematically in Fig. 4. The angle between the primary x-ray beam and the observed x-ray fluorescence beam is 90 deg. To control the two angles, we used a goniometer head which both rotates Rx and Ry. This goniometer is controlled by a computer using a stepper motor and encodcer controller. Rx and Ry rotate through a common center, where the sample is set.

The slits A for the primary x ray are attached to the goniometer Ry and always remain parallel to the sample surface. The incident angle is changed by rotating the goniometer Rx. Since bar A is attached to the goniometer Rx, the bar A pushes the bar B which rotates the slits B when the goniometer Rx moves. Therefore, the slits B also remain parallel to the sample surface. The takeoff angle is changed by rotating the goniometer Ry. In this case, the bar B does not move.

An x-ray generator, with a rotating Mo anode, was op-

Downloaded 05 Aug 2011 to 130.34.134.250. Redistribution subject to AIP license or copyright; see http://rsi.aip.org/about/rights_and_permissions

FIG. 3. The three depth profiles of (a), (b), and (c) are (Au 20 nm/Si), ($Au_{0.6}$10 nm/$Au_{0.4}$10 nm/$Au_{0.35}$10 nm/$Au_{0.25}$10 nm/$Au_{0.2}$10 nm/$Au_{0.1}$20 nm/Si), and ($Au_{0.2}$10 nm/$Au_{0.3}$10 nm/$Au_{0.5}$20 nm/$Au_{0.3}$10 nm/$Au_{0.2}$10 nm/Si), respectively. The Au quantities of the three depth profiles are the same. The IAD-XRF curves of (d)–(f) are calculated from the depth profiles of (a)–(c), respectively. The GIT-XRF curves of (g)–(i) are calculated from the depth profiles of (a)–(c), respectively.

erated at 50 kV and 150 mA. The x-ray fluorescence was measured for several hundred seconds, at each angle, and was analyzed with a multichannel analyzer.

Auger electron spectroscopy (AES) depth profiling was measured with a commercial AES spectrometer (JAMP-7100E; JEOL). Primary electron beam energy of 10.0 kV and

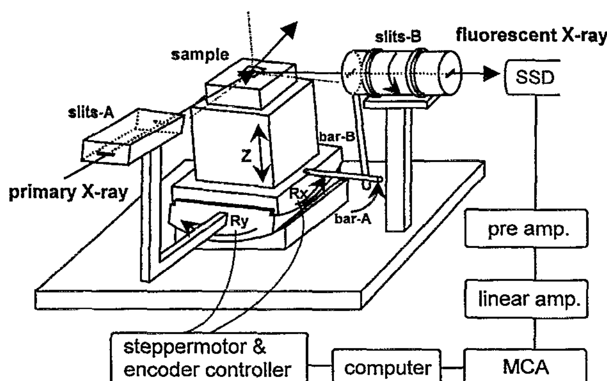

FIG. 4. Experimental setup of the GIT-XRF method.

modulation voltage of 5 $V_{p\text{-}p}$ were used. The sample was etched using 3.0 kV Ar^+ ions.

B. Sample preparation

After the Si wafer (15×15 mm^2) was cleaned in an acetone solution using an ultrasonic cleaner, the oxide layer on the Si wafer was removed by immersion in an HF solution (~50%). Then it was cleaned in a pure water and ethanol solution. A thin Au film was put on the Si wafer by the vacuum evaporation method at a pressure below 1×10^{-4} Pa.

As shown in Fig. 5, the Au/Si sample was then set on a ceramic holder. The sample was heated with a tungsten coil heater to 323, 423, and 523 K for about 30 min. The sample's temperature was controlled with an IR thermometer. After the sample cooled to the room temperature, the GIT-XRF measurement was started.

IV. RESULTS AND DISCUSSIONS

A. Temperature dependence of the GIT-XRF curve

Figure 6 shows the GIT-XRF curves for the Au/Si sample before and after it was heated to 323, 423, and 523 K.

Downloaded 05 Aug 2011 to 130.34.134.250. Redistribution subject to AIP license or copyright; see http://rsi.aip.org/about/rights_and_permissions

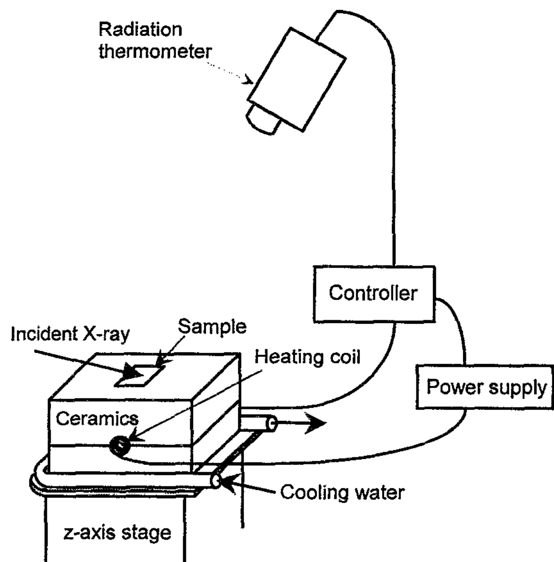

FIG. 5. Schematic drawing of the sample holder to control the temperature of the sample surface.

The takeoff angle of the peak before heating was about 9.5 mrad. This takeoff angle shifts to a lower angle as the temperature of the treatment increases. As a result, the angle for the sample heated to 523 K was about 5.5 mrad. Similar results were reported by Shoji and Hirokawa.[23] This result indicates that the surface density decreases as the temperature increases. In addition, the shape of the experimental curve changes according to temperature. The shape of the curve for the sample before heating was sharp, however, that for the sample heated to 523 K was very broad, and its intensity above 6 mrad was almost constant. The shape of this curve is similar to that for the thick film as shown in Fig. 2(b). Therefore, this result suggests that the distribution width of an Au atom in an Si wafer increases.

Another noteworthy result is the takeoff-angle dependence of the Au $L\alpha$ intensity near the zero angle as shown in Fig. 7(a). Before heating, the Au $L\alpha$ intensity gradually increased from the zero angle. In contrast, it rapidly increases at a critical angle in the case of the sample heated to 523 K.

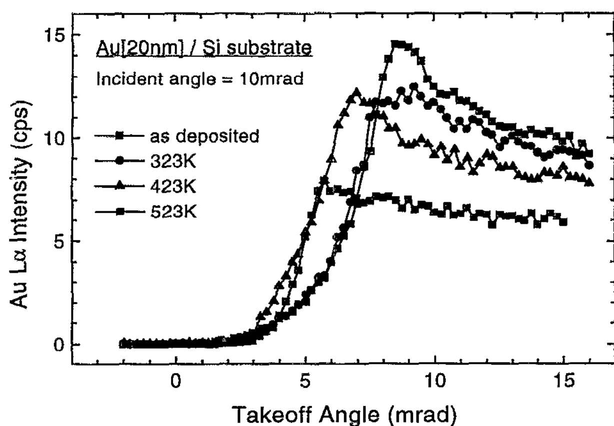

FIG. 6. The temperature dependence of the GIT-XRF curves of the thin Au film (20 nm) on Si.

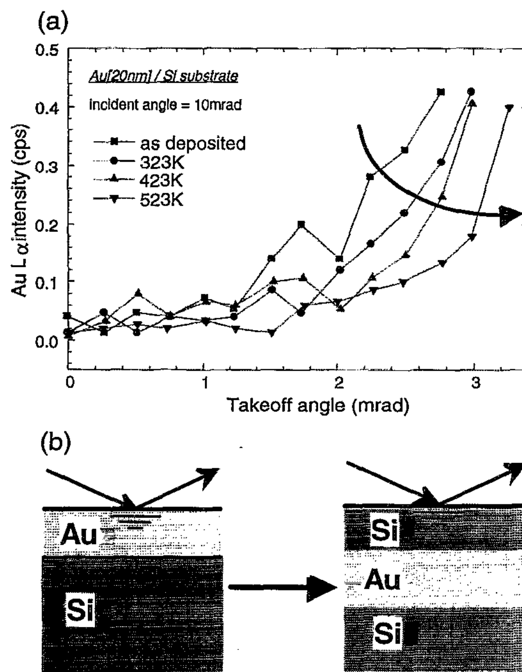

FIG. 7. (a) The expanded GIT-XRF curves near the zero angle. (b) The depth profiles to explain the experimental results of (a).

We explain this result in Fig. 7(b). When the x-ray fluorescence intensity is calculated as a function of the takeoff angle, it is assumed that the x ray which has the same wavelength as the observed x-ray fluorescence irradiates the sample surface according to the reciprocity theorem.[7,12] The takeoff angle shown in Fig. 7(a) is below the critical angle for total reflection, therefore, the total reflection occurs on the Au thin film as shown in the figure on the left-hand side in Fig. 7(b). The observed Au $L\alpha$ intensity below the critical angle is produced by the evanescent wave under the total reflection phenomenon. If Au atoms do not exit near the surface, as shown in the figure on the right-hand side in Fig. 7(b), the Au $L\alpha$ will not be observed below the critical angle. Consequently, the experimental results shown in Fig. 7(a) indicate that the Au layer diffuses into the Si wafer.

B. Depth profiling of the Au/Si heated to 323 and 523 K

After the Au/Si sample was heated to 323 K for about 30 min, the TAD-XRF curves of Au $L\alpha$ were measured at the incident angles of 2, 4, and 6 mrad. These experimental results are shown in Fig. 8(a) with symbols. To explain these experimental results, we overlaid a simulated TAD-XRF curve. The simulated curves which fit best with the experimental plots are shown in fig. 8(a). The calculation model is shown in Fig. 8(b), where the Au (60%)-Si layer exists near the surface, and Au atoms diffuse into the Si to the depth of 50 nm.

The GIT-XRF measurement was performed for the Au/Si sample after heating to 523 K. The TAD-XRF curves at the incident angles of 2, 4, and 6 mrad are shown in Fig. 8(c). The takeoff angles of the peaks shift to about 5.5 mrad, and the shapes of the experimental curves broaden. To explain

Downloaded 05 Aug 2011 to 130.34.134.250. Redistribution subject to AIP license or copyright; see http://rsi.aip.org/about/rights_and_permissions

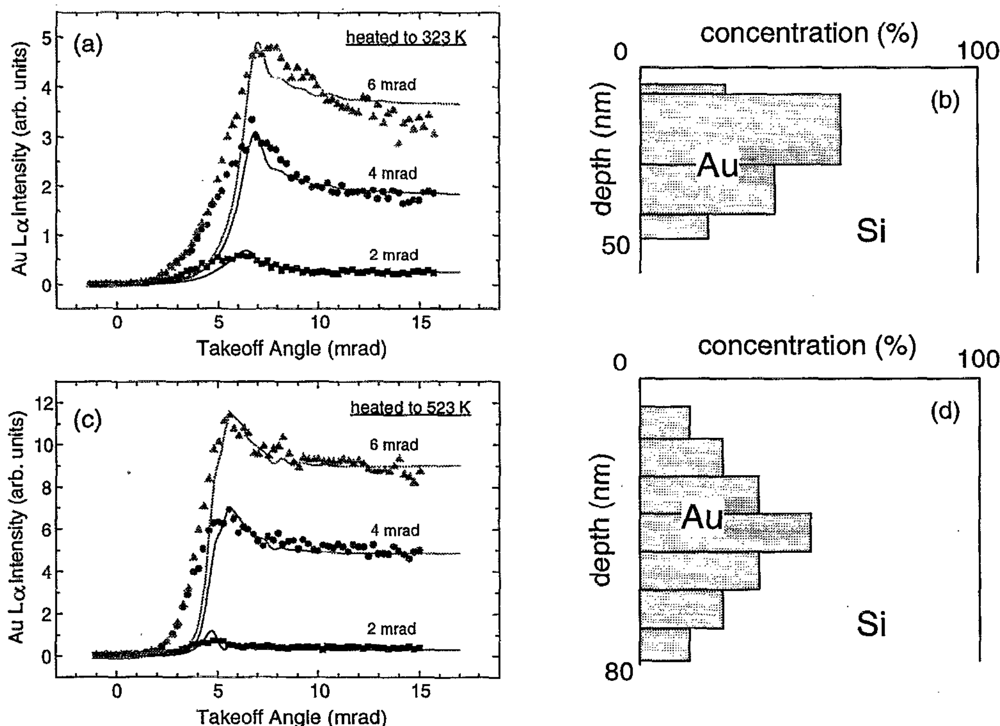

FIG. 8. The experimental GIT-XRF results of the Au/Si sample heated to 323 and 523 K are shown in (a) and (c), respectively. The calculated curves which fit best with the experimental results are also shown with the solid lines. The depth profiles (b) and (d) obtained from the experimental results are (Si 5 nm/$Au_{0.3}$2 nm/$Au_{0.6}$20 nm/$Au_{0.4}$15 nm/$Au_{0.2}$7 nm/S9) and (Si 8 nm/$Au_{0.15}$10 nm/$Au_{0.25}$10 nm/$Au_{0.35}$10 nm/$Au_{0.5}$10 nm/$Au_{0.35}$10 nm/$Au_{0.25}$10 nm/$Au_{0.15}$10 nm/Si), respectively.

these experimental results, we calculated the TAD-XRF curves with the depth profile model shown in Fig. 8(d). The calculated curves are shown in Fig. 8(c). These calculated curves approximate the experimental results. As the temperature raises, the diffusion of Au and Si atoms is accelerated. In the model, the Au concentration reaches its maximum at a depth of about 43 nm, and the range of the Au diffusion is about 80 nm.

C. GIT-XRF and AES depth profiling of Au/Si heated to 423 K

The Au/Si interface reaction has been investigated by using RBS or AES, and it has been determined that a silicon-oxide layer forms on top of the Au layer.[19,20] Since the GIT-XRF measurements were performed in the atmosphere, the x-ray fluorescence from the Si and O atoms could not be measured in this experiment. Thus, the depth profile of the Au/Si sample heated to 423 K was measured by AES using Ar^+ ion sputtering. Figure 9 shows the AES depth profile. The relative concentration was corrected using relative sensitivity factors estimated by the JEOL software. The surface layer was covered by silicon oxide, and Au atoms diffused into the Si.

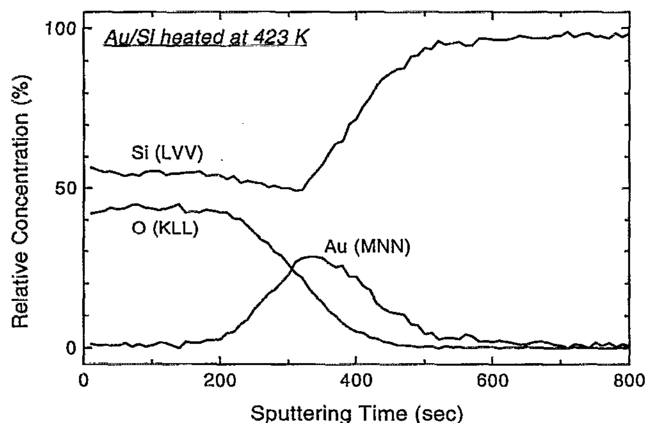

FIG. 9. The AES depth profiles of Au, Si, and O.

Thus, the GIT-XRF result of the Au/Si sample heated to 423 K, shown in Fig. 10(a), was analyzed using a similar depth profile as that obtained by AES. The calculation model and the calculated curves are shown in Figs. 10(b) and 10(a), respectively. The calculated curves approximate the actual experimental results.

DISCUSSION

We have recently developed the GIT-XRF method, and we have found that this method has an advantage for depth profiling in comparison with the angle-dependent TXRF method. The GIT-XRF method was applied for the depth profiling of Au in Si. The GIT-XRF results changed depending on the temperature used in the heat treatment. This means that the GIT-XRF results are sensitive to the change of the depth distribution. However, a perfect fit between the experimental results and the simulated curves could not be obtained. In particular, the incident-angle dependence of the TAD-XRF curves does not agree with the simulated dependence. To overcome this, a monochromatic x-ray beam will

Downloaded 05 Aug 2011 to 130.34.134.250. Redistribution subject to AIP license or copyright; see http://rsi.aip.org/about/rights_and_permissions

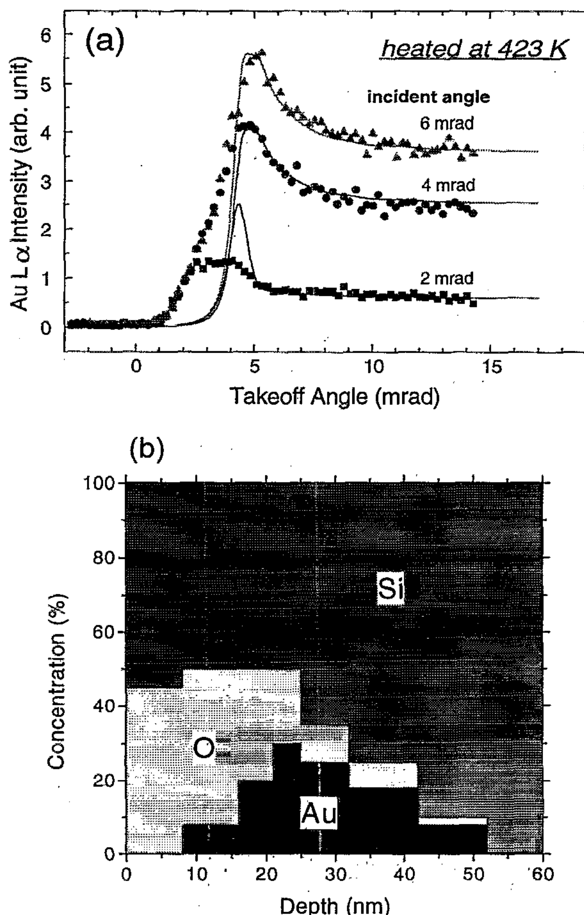

FIG. 10. (a) The experimental GIT-XRF results of Au/Si sample heated to 423 K. (b) The depth profile which fit best with the experimental results. The calculated curves are shown in (a).

be necessary for the primary x ray, because the incident-angle dependence is dependent on the energy of the x ray. We will undertake the experiment and make clear the utility and limitation of the GIT-XRF method.

ACKNOWLEDGMENTS

Parts of this work were supported by a Grant-in-Aid (No. 06650035) from the Ministry of Education, Science and Culture of Japan. We thank Dr. H. Matsuta for cooperation with the AES measurement, and also thank Dr. S. Shucart for helpful discussion.

[1] Y. Yoneda and T. Horiuchi, Rev. Sci. Instrum. **42**, 1069 (1971).
[2] H. Aiginger and P. Wobrauschek, Nucl. Instrum. Methods **114**, 157 (1974).
[3] J. Knoth and H. Schwenke, Fresenius' Z. Anal. Chem. **291**, 200 (1978).
[4] A. Iida, Adv. X-Ray Anal. **34**, 23 (1991).
[5] U. Weisbrod, R. Gutschke, J. Knoth, and H. Schwenke, Appl. Phys. A **53**, 449 (1991).
[6] D. K. G. de Boer, Phys. Rev. B **44**, 498 (1991).
[7] T. Noma, H. Miyata, and S. Ino, Jpn. J. Appl. Phys. **31**, L900 (1992).
[8] P. K. de Bokx and H. P. Urbach, Rev. Sci. Instrum. **66**, 15 (1995).
[9] Y. Sasaki and K. Hirokawa, Appl. Phys. A **50**, 397 (1990).
[10] K Tsuji and K. Hirokawa, Spectrochim. Acta B **48**, 1471 (1993).
[11] K. Tsuji and K. Hirokawa, J. Appl. Phys. **75**, 7189 (1994).
[12] R. S. Becher, J. A. Golovchenko, and J. R. Patel, Phys. Rev. Lett. **50**, 153 (1983).
[13] T. Noma and A. Iida, Rev. Sci. Instrum. **65**, 837 (1994).
[14] K. Tsuji, S. Sato, and K. Hirokawa, Jpn. J. Appl. Phys. **33**, L1277 (1994).
[15] Y. C. Sasaki, Y. Suzuki, Y. Tomioka, and A. Fukuhara, Phys. Rev. B **48**, 7724 (1993).
[16] K. Tsuji, S. Sato, and K. Hirokawa, J. Appl. Phys. **76**, 7860 (1994).
[17] K. Tsuji, S. Sato, and K. Hirokawa, Thin Solid Films (in press).
[18] S. Sato, K. Tsuji, and K. Hirokawa, Appl. Phys. A (in press).
[19] A. Hiraki, E. Lugujjo, and J. W. Mayer, J. Appl. Phys. **43**, 3643 (1972).
[20] A. Hiraki, Jpn. J. Appl. Phys. **22**, 549 (1983).
[21] H. Schwenke and J. Knoth, Adv. X-Ray Chem. Anal. Jpn. **26**, 137 (1995).
[22] G. Wiener, C. Michaelsen, J. Knoth, H. Schwenke, and R. Bormann, Rev. Sci. Instrum. **66**, 20 (1995).
[23] T. Shoji and K. Hirokawa, Surf. Interface Anal. **18**, 773 (1992).

Downloaded 05 Aug 2011 to 130.34.134.250. Redistribution subject to AIP license or copyright; see http://rsi.aip.org/about/rights_and_permissions